

Article

A Comparative Study of Equivalent Circuit Models for Electro-Chemical Impedance Spectroscopy Analysis of Proton Exchange Membrane Fuel Cells

Lei Zhao ^{1,2}, Haifeng Dai ^{1,2,*}, Fenglai Pei ³, Pingwen Ming ^{1,2}, Xuezhe Wei ^{1,2} and Jiangdong Zhou ⁴

¹ School of Automotive Studies, Tongji University, Shanghai 201804, China; 18352861293@163.com (L.Z.); ming_pw@163.com (P.M.); 1911071@tongji.edu.cn (X.W.)

² Clean Energy Automotive Engineering Center, Tongji University, Shanghai 201804, China

³ Shanghai Motor Vehicle Inspection Certification & Tech Innovation Center Co., Ltd., Shanghai 201804, China; 18501473450@163.com

⁴ Nantong Bing Energy Co., Ltd., Nantong 226500, China; zhoujd1203@163.com

* Correspondence: tongjidai@tongji.edu.cn

Abstract: Electrochemical impedance spectroscopy is one of the important tools for the performance analysis and diagnosis of proton exchange membrane fuel cells. The equivalent circuit model is an effective method for electrochemical impedance spectroscopy resolution. In this paper, four typical equivalent circuit models are selected to comprehensively compare and analyze the difference in the fitting results of the models for the electrochemical impedance spectroscopy under different working conditions (inlet pressure, stoichiometry, and humidity) from the perspective of the fitting accuracy, change trend of the model parameters, and the goodness of fit. The results show that the fitting accuracy of the model with the Warburg element is the best for all under each working condition. When considering the goodness of fit, the model with constant phase components is the best choice for fitting electrochemical impedance spectroscopy under different inlet pressure and air stoichiometry. However, under different air humidity, the model with the Warburg element is best. This work can help to promote the development of internal state analysis, estimation, and diagnosis of the fuel cell based on the equivalent circuit modeling of electrochemical impedance spectroscopy.

Keywords: proton exchange membrane fuel cell; electrochemical impedance spectroscopy; equivalent circuit model; comparative study



Citation: Zhao, L.; Dai, H.; Pei, F.; Ming, P.; Wei, X.; Zhou, J. A Comparative Study of Equivalent Circuit Models for Electro-Chemical Impedance Spectroscopy Analysis of Proton Exchange Membrane Fuel Cells. *Energies* **2022**, *15*, 386. <https://doi.org/10.3390/en15010386>

Academic Editor: Li Chen

Received: 2 December 2021

Accepted: 1 January 2022

Published: 5 January 2022

Publisher's Note: MDPI stays neutral with regard to jurisdictional claims in published maps and institutional affiliations.



Copyright: © 2022 by the authors. Licensee MDPI, Basel, Switzerland. This article is an open access article distributed under the terms and conditions of the Creative Commons Attribution (CC BY) license (<https://creativecommons.org/licenses/by/4.0/>).

1. Introduction

With the rapid development of global industrialization, the excessive use of fossil fuels leads to the increasingly serious problem of environmental pollution. In order to reduce the dependence on fossil fuels and environmental pollution, countries around the world are vigorously developing green and sustainable energy [1–3]. Energy storage and conversion technologies are needed to realize the effective utilization of green and sustainable energy. Among them, electrochemical energy technologies such as the lithium-ion battery and the fuel cell are considered to be the most feasible [4,5]. Especially, the proton exchange membrane fuel cell (PEMFC) is attracting more and more attention. Because of its advantages of zero-emission, low noise, and high energy conversion efficiency, it has been applied to many fields, such as fuel cell electric vehicles (FCEV). However, PEMFC is a complex electrochemical system, its performance and durability are still major challenges to large-scale commercialization.

The fuel cell performance is related to the internal state [6–8]. To overcome the challenges mentioned above, it is necessary to use electrochemical diagnostic analysis tools to understand the changes in the internal states of fuel cells [9–11]. As one of the electrochemical diagnostic analysis tools, electrochemical impedance spectroscopy (EIS) has been

widely used in the measurement and diagnosis of electrochemical systems due to its advantages of high accuracy, wide frequency band, simple operation, and no damage [12]. The electrochemical impedance spectroscopy is sensitive to the internal and external conditions of the electrochemical system [13–18]. It can provide general information on kinetics for the electrochemical system [19–21]. Thus, as an effective tool, EIS is often used to study the characteristics of fuel cells or establish the relationship between internal states and operating conditions [22–24].

EIS analysis methods include the equivalent circuit modeling method, physical model method, and relaxation time distribution method, etc. The physical model method is based on the mathematical modeling of the different electrochemical process mechanisms inside the fuel cell to study the impedance characteristics of the system [25]. However, it is difficult to obtain an accurate physical model of the fuel cell [13]. The relaxation time distribution method can extract characteristic time constants from the impedance spectroscopy to distinguish different electrochemical processes without a priori knowledge of the impedance. However, it is difficult to select an appropriate regularization factor required for data processing in this method, and the impedance of each process can be analyzed but difficult to be quantified. The equivalent circuit modeling method is the most commonly used in EIS analysis, the equivalent circuit model is usually composed of basic circuit elements such as series of parallel resistances and capacitance to fit the measured electrochemical impedance spectroscopy. It can combine the internal state of the fuel cell with model parameters to describe the changing trend of the impedance under different working conditions without the complicated mechanism processes. Yan et al. [26] investigated the impedance characteristics of a stack under different operating temperatures with the equivalent circuit model (ECM) and found that high-frequency resistance (HFR) and diameter of the two overlapping arcs gradually decreased with the increase in operating temperatures; Keller et al. [27] experimented to study the EIS sensitivity to relative humidity (RH) of supplied gas in the fuel cell and found that both activation and concentration polarizations increased with the RH of the anode and cathode decreasing. In another study, Malevicha et al. [28] studied the effects of the RH of the anode and cathode on the electrochemically active surface area of the fuel cell.

In addition, the equivalent circuit model can also be used for the fault diagnosis of the fuel cell. Specifically, the fault diagnosis is carried out by measuring the impedance spectroscopy under different working conditions with the auxiliary equipment during the operation, and then using the equivalent circuit modeling method to analyze the model parameters as fault characteristic variables to identify the fault. Rubio et al. [29] established the relationship between the parameters of ECM and the internal states of PEMFC, and realized to diagnose flooding and drying fault of the PEMFC; furthermore, by connecting an inductance element in parallel on the RC circuit, the carbon monoxide poisoning fault of the anode catalyst can be also detected. Through EIS measurement and equivalent circuit modeling, Legros et al. [30] found that PEMFC flooding mainly affected the mass transfer impedance and cathode Warburg impedance, and further proved the feasibility of using EIS for flooding fault diagnosis by acoustic emission technology. Kurz et al. [31] and Kadyk et al. [32] both effectively diagnosed the flooding and membrane drying of the fuel cell based on the equivalent circuit models, and the former further concluded that the virtual part of the fuel cell impedance at 0.5 Hz, and the real part of the impedance at 1 kHz, could distinguish the flooding and membrane drying.

Whether it is internal state analysis or fault diagnosis of the fuel cell, the premise and key point of analysis based on the equivalent circuit modeling method is to establish an accurate equivalent circuit model to describe the electrochemical process of fuel cells. Now, there are many articles based on the equivalent circuit modeling method. However, the equivalent circuit models used by them are different, and the comparative analysis of the performance and applicability of different models in a comprehensive way is still lacking. As a result, there is no great progress in the development of the equivalent circuit model. Therefore, this paper makes a systematical comparison of the performance and

applicability of four typical equivalent circuit models for the first time, and studies the fitting accuracy of each model under different working conditions, the changing trend of the model parameters with the changes in external working conditions and the goodness of fit (GOF) in depth. The work presented in this paper can effectively promote the application of the equivalent circuit model in the state analysis, estimation, and diagnosis of the fuel cell.

2. Experimental Setup

2.1. Testing System

The fuel cell test system (Scribner Associates 850e) consists of the hydrogen supply system, air supply system, fuel cell test bench, fuel cell monomer, back pressure device and so on, as shown in Figure 1. Among them, the hydrogen supply system and air supply system provide hydrogen and oxygen for fuel cells, respectively. The fuel cell test bench can adjust the temperature, humidity, and gas flow of the fuel cell, and monitor the voltage, current, and impedance, etc. At the same time, with the help of the backpressure device, it can further accurately control the anode and cathode inlet pressure of the fuel cell. In the presented research, the commercial membrane electrode assembly (MEA) produced by Qunyi Energy Co., Ltd. is composed of Nafion 212 membranes, a gas diffusion layer composed of the carbon fiber paper and catalyst layer with the platinum loadings of 0.3 in the cathode and 0.1 mg cm^{-2} in the anode. The Pt catalyst is supported by carbon and the thickness of the catalyst layer is $15 \text{ }\mu\text{m}$. The active area is 25 cm^2 . The bipolar plate is a metal composite bipolar plate, which is composed of a thin metal plate and expanded graphite. The flow field is the type of snake channel formed by the stamping method.

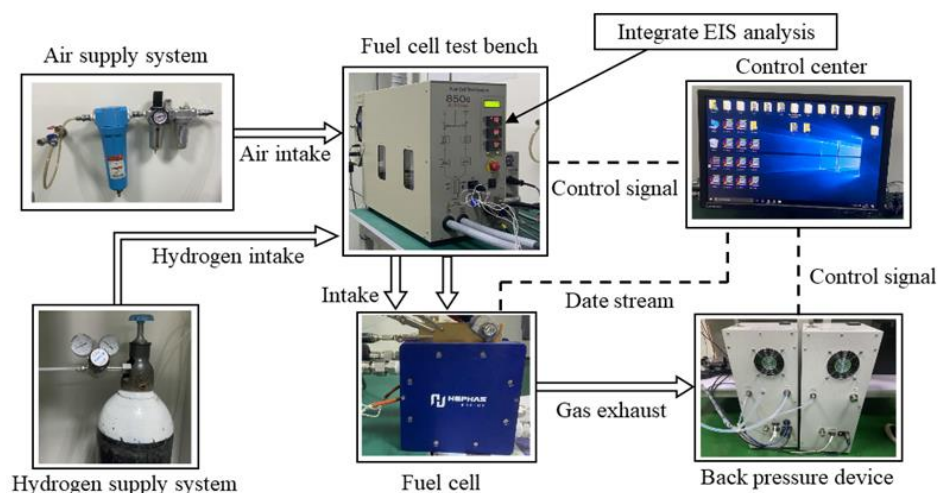


Figure 1. Connection diagram of the fuel cell test system.

2.2. Experiment Procedures and EIS Measurements

During the experiment, the fuel cell was activated first, and then adjusted to the working conditions. The activation procedure is as follows: the current density of fuel cell is increased from 100 to 1700 mA/cm^2 under the optimal operating condition (operation temperature: $75 \text{ }^\circ\text{C}$, cathode/anode inlet pressure: $110/130 \text{ kPa}$, cathode/anode stoichiometry: $2/1.5$, cathode/anode stoichiometry humidity: $50\%/50\%$), and then the current density is reduced to 100 mA/cm^2 with the step of 100 mA/cm^2 . The fuel cell is operating at each current density for 20 min , except for 60 min at 1700 mA/cm^2 . This cycle continues until there is no significant change in the fuel cell performance. The specific parameter settings including cathode/anode inlet pressure, operation temperature, air stoichiometry, and humidity under each working condition are shown in Table 1. In the measurement process, the electrochemical impedance spectroscopy will be measured under the current density of $0.6 \text{ A}\cdot\text{cm}^{-2}$ after the fuel cell maintains a stable operation for 300 s . In order to avoid the impact of the last test on the next test, nitrogen purging is carried out after each test is

completed. In essence, impedance measurement of the fuel cell is the ratio of the voltage to the current, and needs to meet the assumption of the linear change, which requires that the amplitude of disturbance excitation during impedance measurement must be small enough. However, if the amplitude is too small, the noise will affect the accuracy of the measurement. Therefore, the amplitude of the AC is chosen for 8% of the DC in this paper, and the EIS were recorded by sweeping frequencies over the range of 10 kHz to 0.1 Hz, with 10 points per decade.

Table 1. The working conditions of the experiment.

Condition	Cathode/Anode Inlet Pressure, kPa	Operation Temperature, °C	Air Stoichiometry	Air Humidity, %
Different inlet pressure	40/60	75	2	50
	60/80	75	2	50
	80/100	75	2	50
	100/120	75	2	50
	130/150	75	2	50
Different air stoichiometry	110/130	75	1.5	50
	110/130	75	1.7	50
	110/130	75	2	50
	110/130	75	2.5	50
	110/130	75	3	50
Different air humidity	110/130	75	2	10
	110/130	75	2	30
	110/130	75	2	60
	110/130	75	2	80
	110/130	75	2	100

Notes: Hydrogen stoichiometry and humidity is 1.5 and 50% in the experiment, respectively.

Typical electrochemical impedance spectroscopy of the fuel cell is shown in Figure 2. It starts from a certain point on the real axis, followed by two semicircles and a diagonal line, viewed from left to right (high to low frequency). The high-frequency intercept (the point where the real axis intersects the impedance spectroscopy) reflects the ohmic resistance, two semicircles corresponding to the anode and cathode reflect the activation loss caused by a redox reaction in turn, and the low-frequency arc mainly reflects the mass transfer loss of oxygen in the catalyst layer and gas diffusion layer [24,33]. Usually, the ultrahigh-frequency (UHF) band (>2.5 kHz) reflects the inductive reactance characteristic, it may be related to the interference of the electrochemical impedance spectroscopy tester and the cable connected with various external equipment. In addition, according to the literature [34], the inductive reactance also appears in the ultralow frequency (ULF) band, which is related to the adsorption of impurities or the formation of intermediates. The reasons for the formation are complex. However, the frequency of this test is up to 0.1 Hz, and the inductive reactance characteristic of the ultralow frequency band is not obvious. In this paper, both high-frequency and low-frequency inductance are ignored.

Because fuel cells are often compared using the current density rather than current, Area specific resistance (ASR) is used to indicate the equivalent impedance, the unit is $\Omega \cdot \text{cm}^2$, which makes it easier to compare different areas of cells.

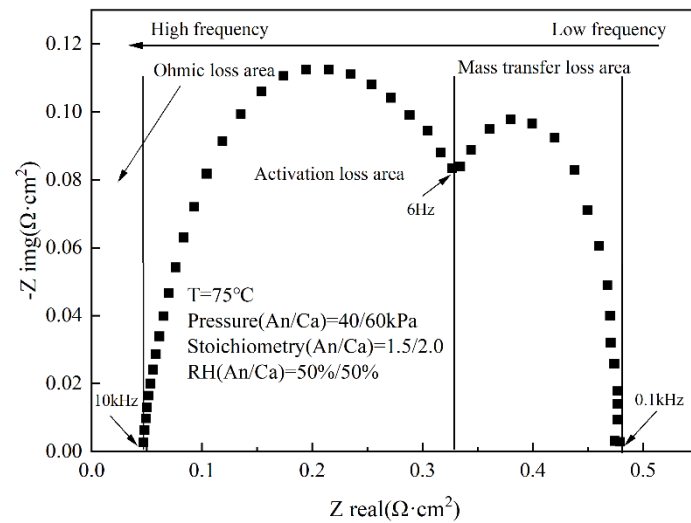


Figure 2. Nyquist diagram of the test fuel cell at 0.6 A/cm².

3. Model Structures

Equivalent circuit models normally consist of resistances, capacitances, constant phase elements, inductors, and Warburg elements. These models are phenomenon-based and are extensively used in electrochemical systems. In general, four typical ECMs have been reported in the literature to interpret electrochemical impedance spectroscopy. The description of these models is shown in Figure 3.

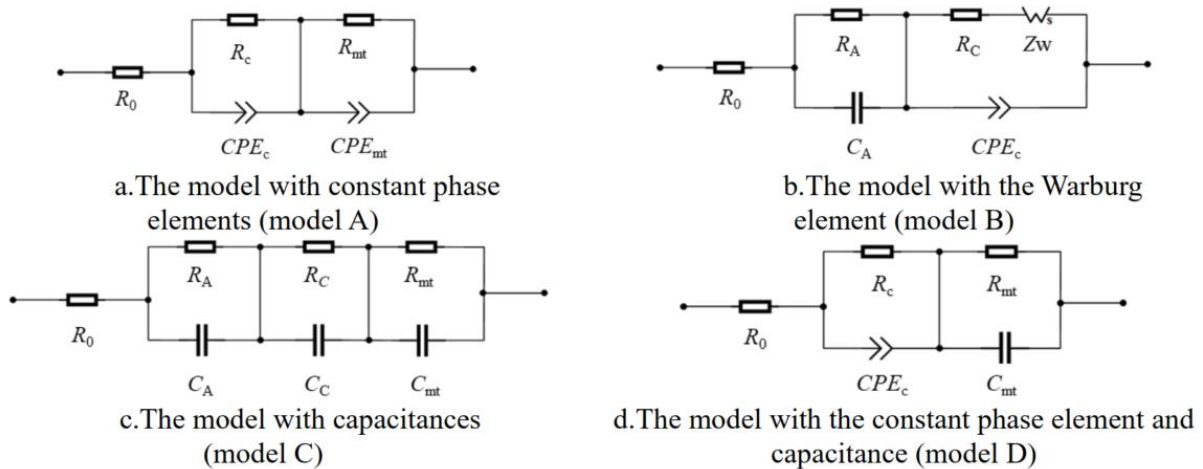


Figure 3. Typical equivalent circuit models used to fit the EIS data of PEMFCs: (a) the model with constant phase elements; (b) the model with the Warburg element; (c) the model with capacitances; (d) the model with the constant phase element and capacitance.

(1) The model with constant phase elements (hereafter referred to as model A) consists of three circuits in series. The first circuit is resistance R_0 . The second and third circuits are the same, both of which are resistance and constant phase element in parallel. R_C and CPE_C in parallel reflect the cathodic activation loss, where R_C represents the resistance of charge transfer caused by the oxygen reduction reaction (ORR), the CPE_C is related to the electrochemical process in the cathode with a rough catalyst layer and uneven catalyst distribution [35], which is expressed by the following formula:

$$Z_{CPE_c} = \frac{1}{T_{CPE_c}(j\omega)^\varphi} \tag{1}$$

where T_{CPE_C} is the term of distributed capacitance, φ is a constant which is lower than 1. CPE_C is equivalent to the capacitance when $\varphi = 1$.

R_{mt} and CPE_{mt} are parallel to describe the mass transfer loss. R_{mt} is the resistance of mass transfer of oxygen diffusion in the catalyst layer. In this model, it is considered that the anode activation loss is very small and can be ignored [26].

(2) The model with the Warburg element (hereafter referred to as model B) consists of a serial resistance, an anode model, and a cathode model. R_0 represents the sum of proton and electron transport resistances in the fuel cell. The anode model includes the charge transfer resistance of the hydrogen oxidation reaction (HOR), R_A , and the capacitance of the catalyst layer, C_A . The cathode model includes charge transfer resistance of the oxygen reduction reaction, R_C , a constant phase element CPE_C , and a finite length Warburg diffusion element, Z_W . Z_W relates to the mass transfer loss in the gas diffusion layer, including the resistance of the gas diffusion layer R_d and the time constant $T_d = l^2/D$, which is given by the following formula [13]:

$$Z_W = \frac{R_d \tanh(j\omega T_d)^p}{(j\omega T_d)^p} \quad (2)$$

where l is the effective diffusion thickness, D is the effective diffusion coefficient of reactants, and $0 < p < 1$ is a constant.

(3) The model with capacitances (hereafter referred to as model C) consists of three parallel RC circuits and a resistance in series, where the first two RC circuits correspond to the activation loss of the anode and cathode. Compared to the model with constant phase elements, capacitances are used instead of the constant phase element in this circuit. The third RC circuit is related to the mass transfer loss of the fuel cell, the impedance elements are R_{mt} and C_{mt} . R_0 is used to describe the resistance of the membrane or electrolyte.

(4) The model with the constant phase element and capacitance (hereafter referred to as model D) is composed of three circuits. This model is similar to the model with constant phase elements in that both activation and mass transfer loss of the anode in the fuel cell is ignored. However, a slight difference is that the resistance and capacitance in parallel in model A are used to describe the cathodic mass transfer loss of the fuel cell, while model D uses the resistance and constant phase element in parallel to describe that.

In this paper, ZView software developed by Scribner Associates Inc in North Carolina, USA is used to fit the measured electrochemical impedance spectroscopy based on different equivalent circuit models. Consider that the units of model parameters are different. To compare and analyze the changes in the model parameters with the changes in the external working conditions, the normalization method will be adopted in this paper, which is given by the following formula:

$$K = \frac{x_i - \bar{x}}{\bar{x}} \% \quad (3)$$

where K is the normalization parameter, x_i is the value of the model parameter, \bar{x} is the average value of the corresponding model parameter.

4. Results and Discussion

The EIS of the fuel cell under different inlet pressure, air stoichiometry, and humidity are measured through the experiment. The four typical equivalent circuit models are selected for comprehensive comparison and analysis from the perspective of the fitting accuracy under different working conditions, the changing trend of the model parameters with the changes in external working conditions, and the goodness of fit.

Furthermore, the chi-square test is used to evaluate the fitting accuracy of each equivalent circuit model. It can show the deviation between the measured value of the electrochemical impedance and the model value. If the chi-square value is larger, the deviation

degree will be greater; otherwise, the deviation will be smaller. The calculation formula of the chi-square test is as follows:

$$\chi^2 = \sum \frac{(f_0 - f_e)^2}{f_e} \quad (4)$$

where f_0 is the measured value of the electrochemical impedance, and f_e is the calculation value of the equivalent circuit model.

4.1. Fitting Accuracy of the Models

4.1.1. Comparison under Different Inlet Pressure

The fitting results of the equivalent circuit models under different inlet pressures are shown in Figure 4. It can be seen that the electrochemical impedance spectroscopy of the fuel cell is sensitive to the change in inlet pressure. On the premise of keeping the inlet pressure difference between cathode and anode unchanged, with the increase in the inlet pressure, the ohmic impedance in the high-frequency region remains unchanged. However, the activation and mass transfer impedances decrease significantly. This is mainly because with the increase in the inlet pressure, the partial pressure of hydrogen and oxygen also increases. According to formula 5, the increase in the molar concentration of reactants in the catalyst layer can improve the exchange current density of the fuel cell, thus improving the kinetic characteristics.

$$j_0 = nFc_R^*f_1 \exp[-\Delta G^{++}/(RT)] \quad (5)$$

where n is the number of electrons transferred in the reaction, F is the Faraday constant, c_R^* is the concentration of reactants at the three-phase interface of the catalyst layer, f_1 is the rate at which the reactants decay to the product, ΔG^{++} represents the change in Gibb's free energy, R is the gas constant, and T is the temperature.

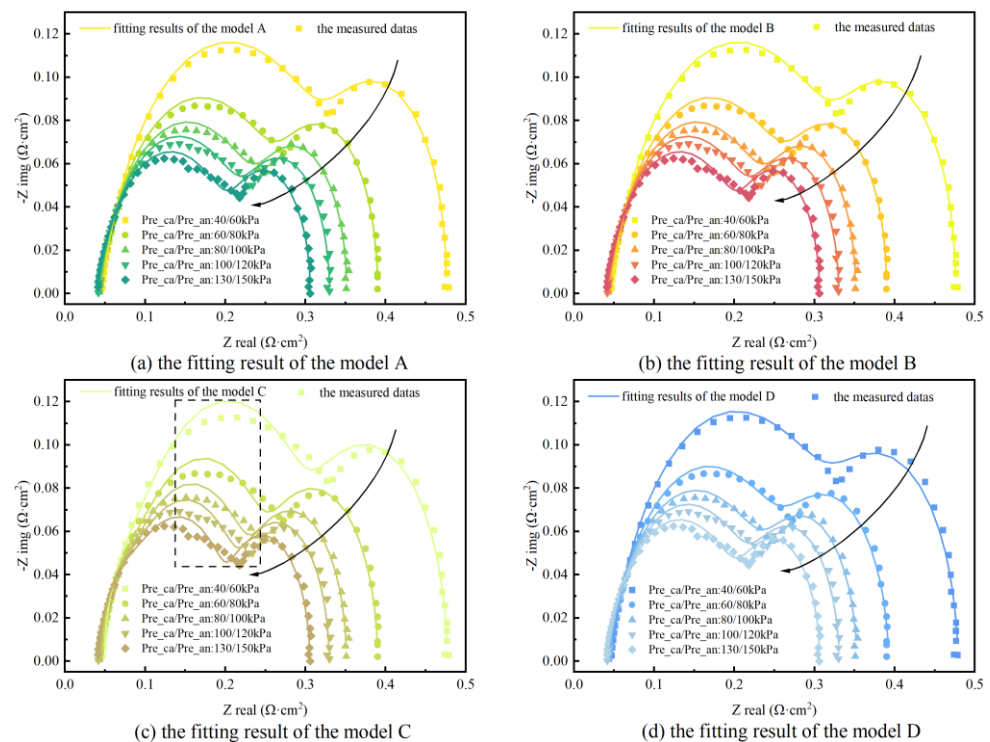


Figure 4. The model-fitting results under different inlet pressure: (a) the fitting result of the model A; (b) the fitting result of the model B; (c) the fitting result of the model C; (d) the fitting result of the model D.

In addition, the mass transfer in the flow channels is improved with the increase in inlet pressure, which is beneficial to overcome the adhesion effect in the porous medium, and accelerate the diffusion of the reaction gas.

The equivalent circuit models fit the measured impedance well. However, the fitting results of model C deviate slightly from the measured data near the middle frequency compared to other models. The main reason is that the middle frequency impedance is related to the electrochemical process of the catalyst layer in the fuel cell, and the charge distribution on the surface of the catalyst layer is not uniform. The capacitance used in model C cannot describe the charge state accurately. Therefore, a constant phase element is used instead of capacitance in some papers.

Further, Table 2 shows the chi-square values of the model fitting results under different inlet pressure. It can be seen that the chi-square values are around 10^{-3} , which shows a good fitting result. In the four equivalent circuit models, the fitting accuracy of model A and model D are the same, and the difference between them is only 0.8%. Model B has the highest fitting accuracy, which is 24.7% higher than that of model C. It is generally considered that the contribution of the anode activation to the impedance is negligible due to the fast HOR kinetics [36]. Therefore, the anode model is not considered in the model A and D. However, D. Malevich et al. [37] also reported that the charge transfer resistance and diffusion resistance of the electrochemical reaction at the anode cannot be ignored when the fuel cell operates at a current density of $0.6 \text{ A}\cdot\text{cm}^{-2}$. Perhaps, for this reason, model B with the anode activation loss has the best fitting result.

Table 2. Chi-square values of the model fitting results under different inlet pressure.

Number	Inlet Pressure	Model A	Model B	Model C	Model D
1	40/60 kPa	1.44×10^{-3}	1.49×10^{-3}	1.70×10^{-3}	1.43×10^{-3}
2	60/80 kPa	1.81×10^{-3}	1.26×10^{-3}	2.03×10^{-3}	1.82×10^{-3}
3	80/100 kPa	1.94×10^{-3}	1.34×10^{-3}	2.20×10^{-3}	1.96×10^{-3}
4	100/120 kPa	2.23×10^{-3}	1.54×10^{-3}	2.52×10^{-3}	2.26×10^{-3}
5	130/150 kPa	1.46×10^{-3}	2.32×10^{-3}	2.09×10^{-3}	1.48×10^{-3}

4.1.2. Comparison under Different Air Stoichiometry

Figure 5 shows the fitting results of each equivalent circuit model under different air stoichiometry. Air stoichiometry has a significant impact on the mass transfer impedance of the fuel cell. With the decrease in air stoichiometry, the liquid water formed at the cathode cannot be completely blown away, which affects the oxygen transport in the gas diffusion layer, increasing mass transfer loss. It can be found from the figure that the low-frequency arc becomes larger gradually as the air stoichiometry decreases. Meanwhile, the decrease in air stoichiometry leads to the decrease in oxygen molar concentration in the catalyst layer and the increase in activation loss, and the overall ohmic impedance changes little.

Model A–D can fit the measured data of the electrochemical impedance well. However, it can also be seen that the fitting accuracy of model C in the middle frequency needs to be improved. This can also be verified by the chi-square test of four equivalent circuit models under different air stoichiometry. The chi-square values of the fitting results of four equivalent circuit models under different air stoichiometry are shown in Table 3. The average chi-square values of the fitting results corresponding to A–D are 1.86×10^{-3} , 1.71×10^{-3} , 2.22×10^{-3} , 1.88×10^{-3} , respectively. It can be seen that the fitting accuracy of model B is the best and that of model C is the worst. The main reason is that air stoichiometry can not only affect the mass transfer process of the fuel cell, but also can affect the activation process. For the activation loss of the fuel cell, a constant phase element compared to a capacitance can more accurately reflect the electrochemical reaction process in the fuel cell. Moreover, the anode activation loss has a certain influence on the measurement results in this experiment; therefore, model B can better fit the measurement data. The chi-square values of model A and model D are almost the same under the same

air stoichiometry. The difference between model A and model D is that model A uses a constant phase element for the mass transfer process, while model D uses a capacitance.

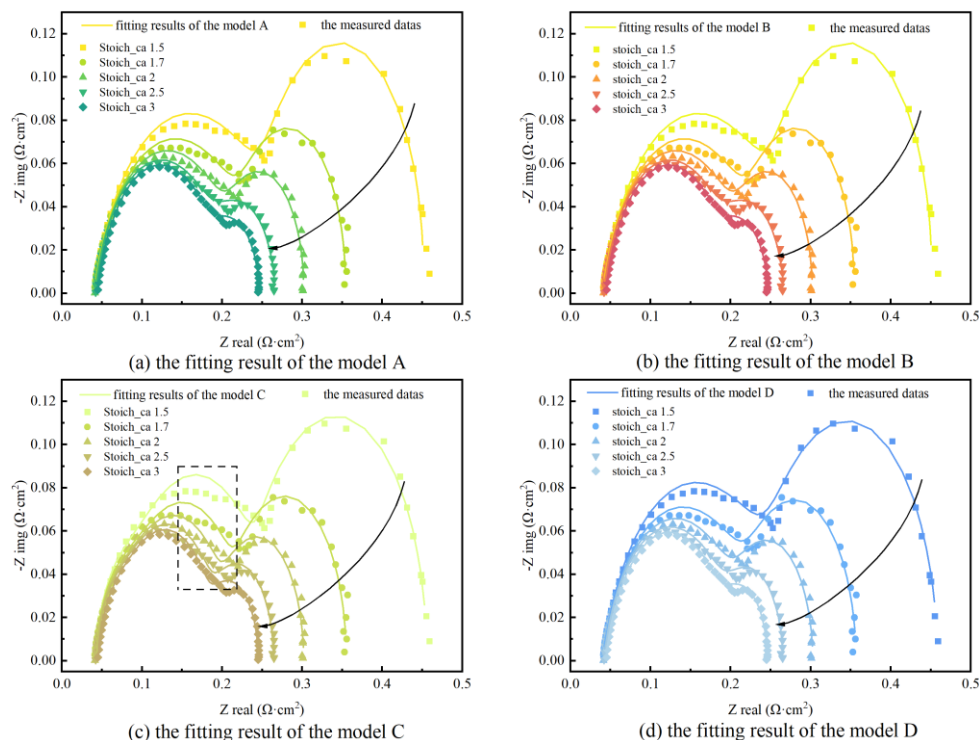


Figure 5. The model-fitting results under different air stoichiometry: (a) the fitting result of the model A; (b) the fitting result of the model B; (c) the fitting result of the model C; (d) the fitting result of the model D.

Table 3. Chi-square values of the model fitting results under different air stoichiometry.

Number	Air Stoichiometry	Model A	Model B	Model C	Model D
1	1.5	1.31×10^{-3}	1.18×10^{-3}	2.08×10^{-3}	1.42×10^{-3}
2	1.7	1.40×10^{-3}	1.10×10^{-3}	1.97×10^{-3}	1.40×10^{-3}
3	2	2.42×10^{-3}	2.71×10^{-3}	2.63×10^{-3}	2.39×10^{-3}
4	2.5	2.23×10^{-3}	1.50×10^{-3}	2.35×10^{-3}	2.25×10^{-3}
5	3	1.92×10^{-3}	2.06×10^{-3}	2.07×10^{-3}	1.93×10^{-3}

4.1.3. Comparison under Different Air Humidity

The fitting results of each equivalent circuit model under different air humidity are shown in Figure 6. It is found that the high-frequency intercept with the real axis and the impedance in middle and low-frequency regions gradually decreases when the air humidity varies from 10% to 80%. The main reason is that the conductivity of the membrane in the fuel cell is related to the water content in the membrane, as the air humidity increases, the water content in the membrane increases; thus, the conductivity of the membrane will increase and the ohmic resistance will decrease. In addition, the electrochemically active surface area (ESA) of the fuel cell is a function of the cathode humidity. The decrease in air humidity leads to a decrease in ESA and an increase in the difficulty of the cathode electrochemical reaction [28]. However, the air humidity is not as large as possible. Usually, 100% air humidity will cause excess water to block the flow channel and the pores of the diffusion layer. If it cannot be removed in time, flooding will occur. This may cause the increase in charge transfer loss and mass transport loss.

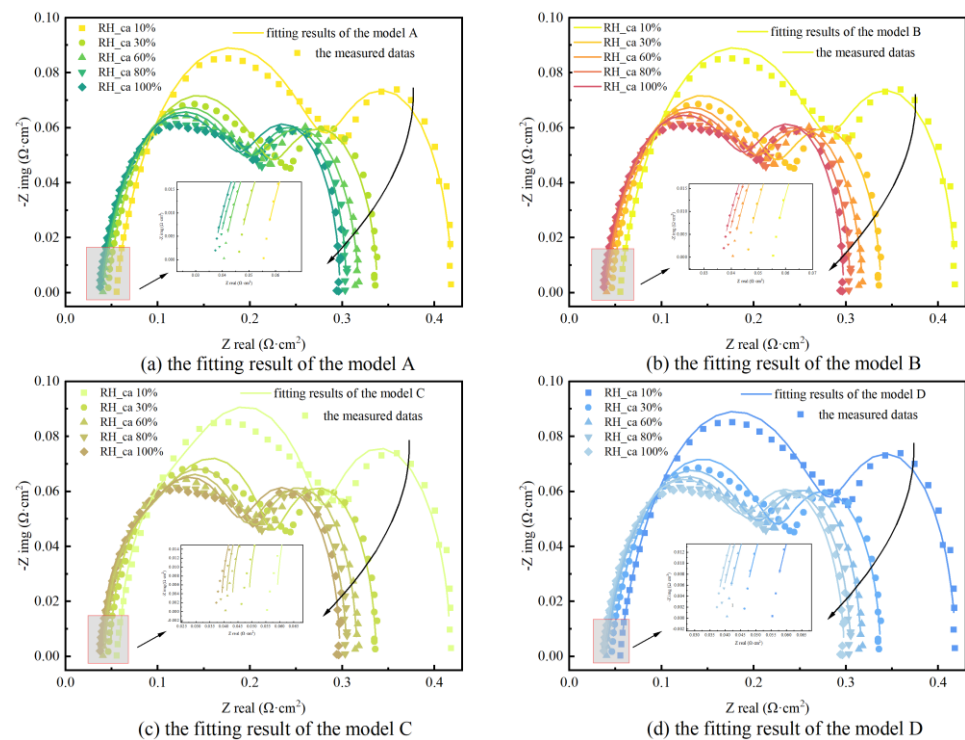


Figure 6. The model-fitting results under different air humidity: (a) the fitting result of the model A; (b) the fitting result of the model B; (c) the fitting result of the model C; (d) the fitting result of the model D.

The fitting values of four equivalent circuit models and measured values under different air humidity are very close, especially model B. According to the chi-square values of the four equivalent circuit models under different air humidity listed in Table 4, the minimum average chi-square value is 1.37×10^{-3} from model B, which indicates that the fitting data of model B are most close to the measured data. The average chi-square values of other models are 2.06×10^{-3} , 2.35×10^{-3} and 2.07×10^{-3} , respectively, corresponding to model A, model C, and model D. According to the literature [38], if the chi-square value of the model is lower than 1×10^{-2} , the fitting accuracy of the model is within the acceptable range. The fitting accuracy of the four models meets the above conditions. It can also be found that the fitting accuracy of model A and model D is still similar under different air humidity, and that of model C is the worst. Because the interface inside the fuel cell is actually in a non-ideal state that cannot be described by the capacitance. This indicates that the fitting accuracy of the model is related to the structure of the model, and has nothing to do with the external working conditions.

Table 4. Chi-square values of the model fitting results under different air humidity.

Number	Air Humidity	Model A	Model B	Model C	Model D
1	10%	2.50×10^{-3}	1.60×10^{-3}	2.78×10^{-3}	2.53×10^{-3}
2	30%	2.02×10^{-3}	1.26×10^{-3}	2.35×10^{-3}	2.05×10^{-3}
3	60%	2.42×10^{-3}	1.57×10^{-3}	2.59×10^{-3}	2.42×10^{-3}
4	80%	1.59×10^{-3}	1.13×10^{-3}	2.01×10^{-3}	1.61×10^{-3}
5	100%	1.74×10^{-3}	1.30×10^{-3}	2.00×10^{-3}	1.77×10^{-3}

4.2. The Model Goodness of Fit

In general, the fitting accuracy of the model increases with the increase in the model complexity, but it also brings a common problem of overfitting when the model is too complex. Therefore, the key point of the model selection is to find the optimal balance between the complexity and fitting accuracy. Akaike information criterion (AIC) is a

standard to measure the model goodness of fit. It comprehensively evaluates the complexity of the model and accuracy of the fitting results by adding a penalty term of the model complexity. It is given by the following formula [39]:

$$AIC = 2k + n \ln(SSR/n) \quad (6)$$

where k is the number of model parameters, n is the number of data samples, and SSR is the residual sum of squares.

As the complexity of the model increases, the AIC value decreases, but when the complexity continues to increase, and the accuracy cannot be further improved significantly, the AIC value will increase. Therefore, the goal of the model selection is the smallest AIC.

The complexity of the model is related to the model parameters. The numbers of the parameters in both model A and C are seven, that in model D is six. The number of parameters in model B is at most nine, which means that the complexity of model B is the highest. Average AIC values of the fitting results of the four equivalent circuit models under different inlet pressure, air stoichiometry, and air humidity are listed in Table 5 and compared under the same working condition. It can be seen from the table that the average AIC value of model C is the largest under each working condition, which indicates that the GOF of model C is the worst. This is mainly due to the lowest fitting accuracy of model C. Model B has the highest fitting accuracy. However, it only has the smallest average AIC under different air humidity. The reason is that model B has the most complex structure and the problem of the overfitting occurs under different inlet pressure and air stoichiometry. Meanwhile, compared to model B, the average AIC value of model A is smaller. This indicates that model A is a preferred choice for the electrochemical impedance spectroscopy analysis under different inlet pressure and air stoichiometry. In addition, the average AIC value of model A is slightly smaller than that of model D under the same working condition, mainly because model A and model D have similar structures. Further, from the point of view of the most suitable working conditions for each equivalent circuit model. The average AIC values of the model A and D are the lowest under different inlet pressures. Model B and C have the lowest average AIC value under different air humidity.

Table 5. Average AIC values of the model fitting results under different working conditions.

Working Condition	Model A	Model B	Model C	Model D
Different inlet pressure	−519.91	−503.86	−474.25	−511.27
Different air stoichiometry	−512.26	−506.97	−498.12	−508.70
Different air humidity	−507.06	−508.30	−500.32	−505.64

4.3. Changing Trend of the Model Parameters

4.3.1. Changing Trend under Different Inlet Pressure

Figure 7 shows the parameter variations of the four equivalent circuit models under different inlet pressures. It can be seen from the figure that R_0 , R_C , and R_{mt} in model A and D; R_0 and R_A in model B; and R_0 and R_{mt} in model C gradually decrease with the increase in inlet pressure. The main reason is that when the inlet pressure increases, it is conducive to overcome the adhesion effect in the porous medium and improve the mass transfer. The resistance of mass transfer gradually decreases. Meanwhile, with the increase in inlet pressure, the molar concentration of hydrogen and oxygen increases and improves the electrochemical reaction; thus, the resistance of charge transfer is reduced. However, R_C in model B and R_A and R_C in model C do not show a monotonic relationship with the inlet pressure, which may be related to the structure of the model and the fitting algorithm. In addition, the structure of model A and model D are similar, and the variation range of R_C in model A and model D is almost the same. After normalization, R_C in model A and model D decreases from 34.5% and 32.8% at 40/60 Pa (the left side represents the cathode inlet pressure, and the right side represents the anode inlet pressure) to −21% and −20.23% at 130/150 Pa, respectively.

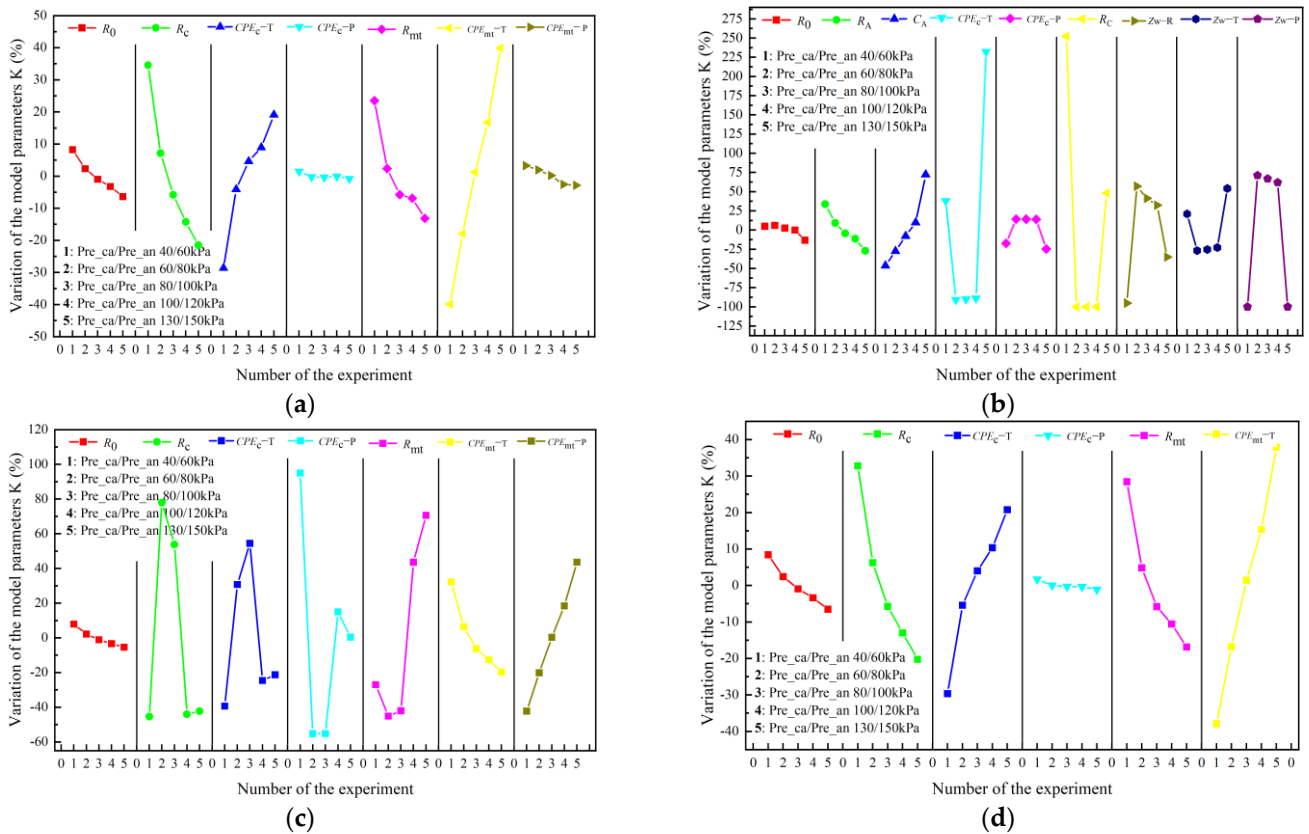


Figure 7. The Changing trend of the model parameters under different inlet pressure: (a) the parameter variations of model A; (b) the parameter variations of model B; (c) the parameter variations of model C; (d) the parameter variations of model D.

At the same time, it can be also found that the CPE_C-T and $CPE_{mt}-T$ in model A, the C_A in model B, the C_{mt} in model C, and the CPE_C and C_{mt} in model D have a linear relationship with the inlet pressure. This is because the redistribution of charge at the interface inside the fuel cell also leads to the change in capacitance. However, due to the complexity of the mechanism of charge transfer and distribution in the fuel cell, the variation in the fitting parameters from the capacitance or constant phase element is random, which needs to be further studied and analyzed.

4.3.2. Changing Trend under Different Air Stoichiometry

When air stoichiometry increases, the air velocity increases and blows away the excess liquid water, thus improving the convection in the channel. The transport capacity of the oxygen in the gas diffusion layer is enhanced, and the resistance of mass transfer is reduced. The parameter variations of each equivalent circuit model under different air stoichiometry are shown in Figure 8. It can be seen from the figure that R_{mt} in model A, R_{mt} in model C, and R_{mt} in model D show a monotonic decreasing trend, and their changing ranges are roughly the same, ranging from 80% to 40%. In addition, R_c in model A, R_A , and R_C in model B, and R_c in model D also show a linear relationship with the air stoichiometry, the reason is that with the increase in air stoichiometry, the molar concentration of oxygen in the catalyst layer increases, and the resistance of charge transfer will decrease. In addition, literature studies have shown that the process of charge transfer in the fuel cell is also affected by mass transfer. Pivac et al. studied the effect of air stoichiometry on the fuel cell and reported similar results [34]. However, the change in resistance of charge transfer is smaller than that of mass transfer. For example, the variation in R_c in model A is 43.9%, while that of R_{mt} is 125.1%. This is also consistent with the fact that the air excess coefficient has a greater influence on the mass transfer loss than the activation loss. For the

fitting parameters from the capacitance or constant phase element, there is also a linear relationship between the CPE_c-T and CPE_c-P in model A and air stoichiometry, and so do these of model D.

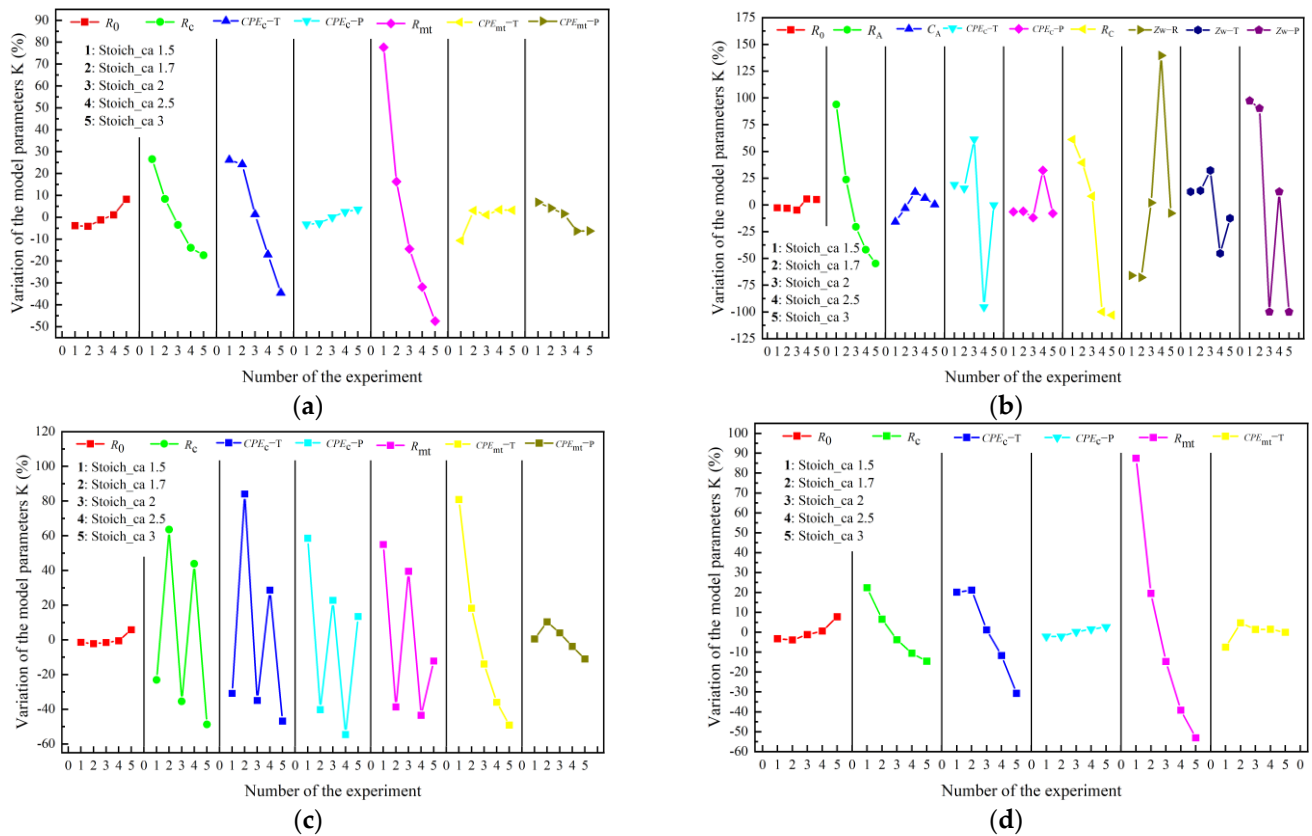


Figure 8. The Changing trend of the model parameters under different air stoichiometry: (a) the parameter variations of model A; (b) the parameter variations of model B; (c) the parameter variations of model C; (d) the parameter variations of model D.

4.3.3. Changing Trend under Different Air Humidity

Figure 9 shows that the parameter change trend of the four equivalent circuit models under different air humidity. It can be seen that R_0 in model A–D gradually decreases with the increase in air humidity. This is because the ohmic resistance is mainly determined by the membrane conductivity. As the air humidity increases, the reaction gas brings more water to the membrane, causing the membrane conductivity to increase. At the same time, the water content in the membrane is beneficial to the transport of the oxygen; therefore, the R_{mt} in the model A and D, and $Zw-T$ in the model B gradually decrease as the air humidity increases. However, the higher water content in the membrane will cause flooding of the gas diffusion layer and increase oxygen transport resistance. In addition, R_C in model A and R_C in model D also show monotonic decreasing changes with air humidity increasing. The reason is that with the increase in air humidity, the proton mobility is enough to affect the oxygen reduction reaction, which will decrease the resistance of charge transfer in the fuel cell. However, R_A and R_C in the model B and C do not show the monotonic trend. For the fitting parameters from the capacitance or constant phase element, the CPE_c-T in the model A and B has a monotonic trend with the change in air humidity.

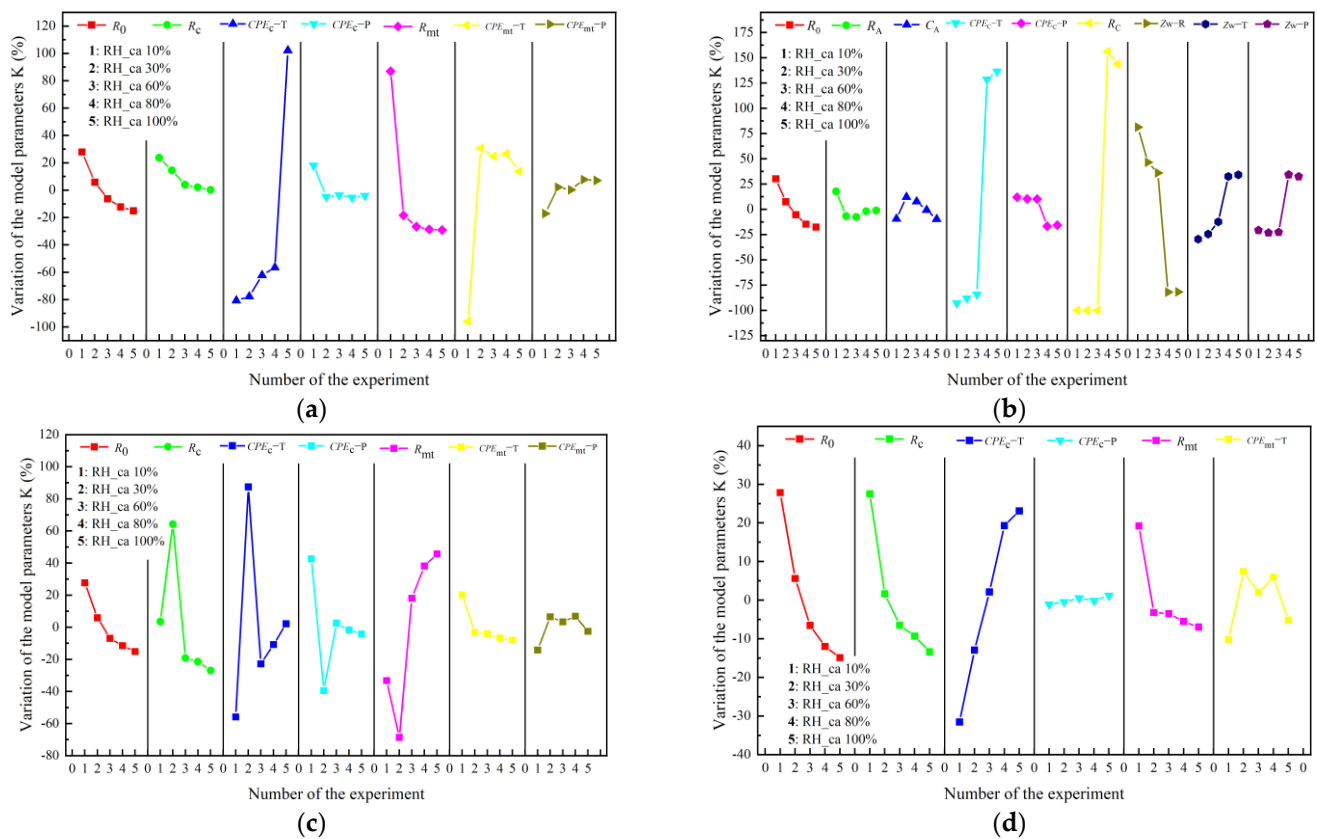


Figure 9. The Changing trend of the model parameters under different air humidity: (a) the parameter variations of model A; (b) the parameter variations of model B; (c) the parameter variations of model C; (d) the parameter variations of model D.

5. Conclusions

In this paper, four typical equivalent circuit models for fitting electrochemical impedance spectroscopy of the fuel cell are comprehensively compared and studied. The impedance data of the fuel cell under different inlet pressure, operation temperature, air stoichiometry, and air humidity are measured through experiment. The fitting accuracy under different working conditions, the changing trend of the model parameters with the changes in external working conditions, and the model goodness of fit are analyzed. The main conclusions are as follows:

(1) The fitting accuracy mainly depends on the model structure. The fitting accuracy of the model with the Warburg element is the best under each working condition, and that of the model with capacitances is the lowest. The fitting accuracy of the model with constant phase elements and the model with the constant phase element and capacitance is the same due to the similar structures.

(2) The model selection should consider not only the fitting accuracy, but also the complexity of the model. AIC was used to comprehensively evaluate the accuracy and complexity of the model. The average AIC value of model A is the lowest under different inlet pressure and air stoichiometry, and under different air humidity, that of model B is the lowest.

(3) Some model parameters in the models tend to show a monotonic trend with the change in the working conditions, but the parameters with monotonic changes are differences between the models, which may be caused by the structure of the model and the fitting algorithm. Therefore, different parameters can be selected to represent the state of the fuel cell for different models.

The above conclusions can provide an important reference for the internal state analysis, estimation, and diagnosis of the fuel cell based on the equivalent circuit modeling analysis.

Author Contributions: Formal analysis, J.Z.; Methodology, P.M.; Project administration, F.P.; Resources, H.D.; Supervision, X.W.; Writing—original draft, L.Z. All authors have read and agreed to the published version of the manuscript.

Funding: This research was funded by National Key Research and Development Program of China grant number 2019YFB1504605 and 2018YFB0106502.

Institutional Review Board Statement: Not applicable.

Acknowledgments: This work was supported by National Key Research and Development Program of China (Funding Number: 2019YFB1504605, 2018YFB0106502).

Conflicts of Interest: The authors declare no conflict of interest.

References

1. Chu, S.; Majumdar, A. Opportunities and challenges for a sustainable energy future. *Nature* **2012**, *488*, 294–303. [[CrossRef](#)] [[PubMed](#)]
2. Tian, N.; Lu, B.; Yang, X.; Huang, R.; Jiang, Y.; Zhou, Z.; Sun, S. Rational design and synthesis of low-temperature fuel cell electrocatalysts. *Electrochem. Energy Rev.* **2018**, *1*, 54–83. [[CrossRef](#)]
3. Zhang, H.; Lu, W.; Li, X. Progress and perspectives of flow battery technologies. *Curr. Opin. Electrochem.* **2019**, *18*, 492–506.
4. Lu, J.; Chen, Z.; Pan, F.; Cui, Y.; Amine, K. High-Performance Anode Materials for Rechargeable Li-thiumIon Batteries. *Electrochem. Energy Rev.* **2018**, *1*, 35–53. [[CrossRef](#)]
5. Ascencio, C.D.; Robles, A.S.; Guerrero, A.H.; Andrade, S.C. Numerical modeling of a proton exchange membrane fuel cell with tree-like flow field channels based on an entropy generation analysis. *Energy* **2017**, *133*, 306.e16. [[CrossRef](#)]
6. Gatto, I.; Carbone, A.; Saccà, A.; Passalacqua, E.; Oldanib, C.; Merlob, L.; Sebastián, D.; Aricò, A.S.; Baglio, V. Increasing the stability of membrane-electrode assemblies based on Aquivion (R) membranes under automotive fuel cell conditions by using proper catalysts and ionomers. *J. Electroanal. Chem.* **2019**, *842*, 59–65. [[CrossRef](#)]
7. Zhou, D.; Gao, F.; Breaz, E.; Ravey, A.; Miraoui, A. Degradation prediction of PEM fuel cell using a moving window based hybrid prognostic approach. *Energy* **2017**, *138*, 1175–1186. [[CrossRef](#)]
8. Yuan, H.; Dai, H.F.; Wei, X.Z.; Ming, P. Model-based observers for internal states estimation and control of proton exchange membrane fuel cell system: A review. *J. Power Sources* **2020**, *468*, 228376. [[CrossRef](#)]
9. Hunsom, M. Electrochemical impedance spectroscopy (EIS) for PEM fuel cells. In *Spectroscopic Properties of Inorganic and Organometallic Compounds: Techniques, Materials and Applications*; Royal Society of Chemistry: London, UK, 2011; Volume 42.
10. St-Pierre, J.; Myers, D.J.; Borup, R.L. Preface-focus issue on proton exchange membrane fuel cell (PEMFC) durability. *J. Electrochem. Soc.* **2018**, *165*, Y7. [[CrossRef](#)]
11. Brunetto, C.; Moschetto, A.; Tina, G. PEM fuel cell testing by electrochemical impedance spectroscopy. *Electr. Power Syst. Res.* **2009**, *79*, 17–26. [[CrossRef](#)]
12. Yuan, X.Z.; Song, C.; Wang, H.; Zhang, J. *Electrochemical Impedance Spectroscopy in PEM Fuel Cells: Fundamentals and Applications*; Springer: London, UK, 2010; Volume 5, pp. 193–262.
13. Macdonald, J.R.; Barsoukov, E. *Impedance Spectroscopy: Theory, Experiment, and Applications*; Wiley: Hoboken, NJ, USA, 2018.
14. Macdonald, D.D. Why electrochemical impedance spectroscopy is the ultimate tool in mechanistic analysis. *ECS Trans.* **2009**, *19*, 55–79. [[CrossRef](#)]
15. Maizia, R.; Dib, A.; Thomas, A.; Martemianov, S. Proton exchange membrane fuel cell diagnosis by spectral characterization of the electrochemical noise. *J. Power Sources* **2017**, *342*, 553–561. [[CrossRef](#)]
16. Lv, J.L.; Liang, T.X.; Wang, C. Comparison of corrosion behavior between coarse grained and nanocrystalline NiFe alloys in chloride solutions and proton exchange membrane fuel cell environment by EIS, XPS and Raman spectra techniques. *Energy* **2016**, *112*, 67–74.
17. Sui, P.C.; Zhu, X. Modeling of PEM Fuel Cell Catalyst Layers: Status and Outlook. *Electrochem. Energy Rev.* **2019**, *2*, 428–466. [[CrossRef](#)]
18. Wang, R.; Wang, H.; Luo, F.; Liao, S. Core-Shell-Structured Low-Platinum Electrocatalysts for Fuel Cell Applications. *Electrochem. Energy Rev.* **2018**, *1*, 324–387. [[CrossRef](#)]
19. Huang, Q.-A.; Hui, R.; Wang, B.; Zhang, J. A review of AC impedance modeling and validation in SOFC diagnosis. *Electrochim. Acta* **2007**, *52*, 8144–8164. [[CrossRef](#)]
20. Li, W.; Huang, Q.-A.; Yang, C.; Chen, J.; Tang, Z.; Zhang, F.; Li, A.; Zhang, L.; Zhang, J. A fast measurement of Warburg-like impedance spectra with Morlet wavelet transform for electrochemical energy devices. *Electrochim. Acta* **2019**, *322*, 134760. [[CrossRef](#)]

21. Yezerska, K.; Liu, F.; Dushina, A.; Sergeev, O.; Wagner, P.; Dyck, A.; Wark, M. Analysis of the regeneration behavior of high temperature polymer electrolyte membrane fuel cells after hydrogen starvation. *J. Power Sources* **2020**, *449*, 227–562. [[CrossRef](#)]
22. Lasia, A. Electrochemical impedance spectroscopy and its applications. In *Modern Aspects of Electrochemistry*; Springer: Boston, MA, USA, 2002; pp. 143–248.
23. Song, J.; Bazant, M.Z. Electrochemical impedance imaging via the distribution of diffusion times. *Phys. Rev. Lett.* **2018**, *120*, 116001. [[CrossRef](#)]
24. Yuan, H.; Dai, H.; Ming, P.; Zhao, L.; Tang, W.; Wei, X. Understanding dynamic behavior of proton exchange membrane fuel cell in the view of internal dynamics based on impedance. *Chem. Eng. J.* **2021**, *431*, 134035. [[CrossRef](#)]
25. Niya, S.M.R.; Phillips, R.K.; Hoorfar, M. Process modeling of the impedance characteristics of proton exchange membrane fuel cells. *Electrochim. Acta* **2016**, *191*, 594–605. [[CrossRef](#)]
26. Yan, X.; Hou, M.; Sun, L.; Liang, D.; Shen, Q.; Xu, H.; Ming, P.; Yi, B. AC impedance characteristics of a 2kW PEM fuel cell stack under different operating conditions and load changes. *Int. J. Hydrogen Energy* **2007**, *32*, 4358–4364. [[CrossRef](#)]
27. Keller, S.; Ozel, T.; Scherzer, A.C.; Gerteisen, D.; Groos, U.; Hebling, C.; Manoli, Y. Characteristic time constants derived from the low-frequency arc of impedance spectra of fuel cell stacks. *Electrochem. Energy* **2018**, *15*, 021002.
28. Malevicha, D.; Halliop, E.; Peppley, B.A.; Pharoah, J.G.; Karan, K. Effect of relative humidity on electrochemical active area and impedance response of PEM fuel cell. *ECS Trans.* **2008**, *16*, 1763–1774. [[CrossRef](#)]
29. Rubio, M.A.; Urquia, A.; Dormido, S. Diagnosis of performance degradation phenomena in PEM fuel cells. *Int. J. Hydrogen Energy* **2010**, *35*, 2586–2590. [[CrossRef](#)]
30. Legros, B.; Thivel, P.X.; Druart, F.; Butletl, Y.; Nogueira, R. Diagnosis and modelling of proton-exchange-membrane fuel cell via electrochemical-impedance-spectroscopy and Acoustic-Emission measurements. In Proceedings of the 2009 8th International Symposium on Advanced Electromechanical Motion Systems & Electric Drives Joint Symposium, Lillie, France, 1–3 July 2009.
31. Kurz, T.; Hakenjos, A.; Krämer, J.; Zedda, M.; Agert, C. An impedance-based predictive control strategy for the state-of-health of PEM fuel cell stacks. *J. Power Sources* **2008**, *180*, 742–747. [[CrossRef](#)]
32. Kadyk, T.; Hanke-Rauschenbach, R.; Sundmacher, K. Nonlinear frequency response analysis of PEM fuel cells for diagnosis of dehydration, flooding and CO-poisoning. *J. Electroanal. Chem.* **2009**, *630*, 19–27. [[CrossRef](#)]
33. Heinzmann, M.; Weber, A.; Ivers-Tiffée, E. Advanced impedance study of polymer electrolyte membrane single cells by means of distribution of relaxation times. *J. Power Sources* **2018**, *402*, 24–33. [[CrossRef](#)]
34. Pivac, I.; Šimić, B.; Barbir, F. Experimental diagnostics and modeling of inductive phenomena at low frequencies in impedance spectra of proton exchange membrane fuel cells. *J. Power Sources* **2017**, *365*, 240–248. [[CrossRef](#)]
35. Jorcin, J.-B.; Orazem, M.; Pébère, N.; Tribollet, B. CPE analysis by local electrochemical impedance spectroscopy. *Electrochim. Acta* **2006**, *51*, 1473–1479. [[CrossRef](#)]
36. Makharia, R.; Mathias, M.; Baker, D.R.; Iaculli, J.; Murphy, M.W. Electrolyte resistance measurement in the catalyst layer of polymer electrolyte fuel cells using electrochemical impedance spectroscopy. *J. Electrochem. Soc.* **2005**, *152*, 298–314. [[CrossRef](#)]
37. Malevich, D.; Halliop, E.; Peppley, B.A.; Pharoah, J.G.; Karan, K. Investigation of Charge-Transfer and Mass-Transport Resistances in PEMFCs with Microporous Layer Using Electrochemical Impedance Spectroscopy. *J. Electrochem. Soc.* **2009**, *156*, B216–B224. [[CrossRef](#)]
38. Ren, P.; Pei, P.; Li, Y.; Wu, Z.; Chen, D.; Huang, S.; Jia, X. Diagnosis of water failures in proton exchange membrane fuel cell with zero-phase ohmic resistance and fixed-low-frequency impedance. *Appl. Energy* **2019**, *239*, 785–792. [[CrossRef](#)]
39. Costanza, R. Model goodness of fit: A multiple resolution procedure. *Ecol. Model.* **1989**, *47*, 199–215. [[CrossRef](#)]